Half-life measurements of several states in ^{95,97}Sr, ^{97,100,104}Zr, ^{106}Mo, and ^{148}Ce

J. K. Hwang,[1] A. V. Ramayya,[1] J. H. Hamilton,[1] Y. X. Luo,[1,2] A. V. Daniel,[3] G. M. Ter-Akopian,[3] J. D. Cole,[4] and S. J. Zhu[1,5]

[1]*Physics Department, Vanderbilt University, Nashville, Tennessee 37235, USA*

[2]*Lawrence Berkeley National Laboratory, Berkeley, California 94720, USA*

[3]*Flerov Laboratory for Nuclear Reactions, JINR, Dubna, Russia*

[4]*Idaho National Laboratory, Idaho Falls, Idaho 83415, USA*

[5]*Department of Physics, Tsinghua University, Beijing 100084, Peoples Republic of China*

(Received 24 August 2005; published 20 April 2006)

Half-lives $T_{1/2}$ of states in ^{95,97}Sr, ^{97,100,104}Zr, ^{106}Mo, and ^{148}Ce, which decay by delayed γ transitions, were determined by using a new time-gated triple γ coincidence method. Transition energy dependent effects such as time walks, time jitters, amplitude walks, and possible timing fluctuations of Ge detectors that contribute to the width of the time window were taken into consideration by comparing prompt and delayed cascades with similar transition energies. It is shown that the normalized triple γ coincidence counts of two prompt cascades with similar transition energies are similar. Also, it is observed that the real triple γ coincidence counts in the prompt cascades change systematically with the widths of the coincidence time window and the transition energies. Half-lives of states in ^{100,104}Zr were measured for the first time. The half-lives of states in the delayed cascades were determined by using the prompt cascades with transition energies similar to those in delayed cascades. The half-life of the 2^+ state in ^{104}Zr is measured to be 2.0(3) ns. The $B(E2; 2^+ \rightarrow 0^+)(e^2\,b^2)$ value and quadrupole deformation β_2 are 0.40(6) $(e^2\,b^2)$ and 0.47(7), respectively. ^{104}Zr has the most deformed 2^+ state among medium and heavy even-even nuclei, except for ^{102}Sr. This method is only approximately valid, but it is believed to be generally within 10% of the true value.

DOI: 10.1103/PhysRevC.73.044316 PACS number(s): 21.10.Tg, 25.85.Ca, 27.60.+j, 29.30.Kv

I. INTRODUCTION

Half-life $T_{1/2}$ measurements of nuclear states have been a major source of information on nuclear deformations, shell structures, and validity of nuclear models. Previously, half-lives of several states in neutron-rich nuclei were determined by measuring singles γ spectra as a function of time or from γ-γ coincidence spectra with isotopes produced in the fission of ^{235}U, ^{239}Pu, ^{248}Cm, and ^{252}Cf. Most of the previous results were obtained by using the separated isotopes produced in the fission of these nuclei. Numerous level half-lives were also determined from the β-γ, α-γ, and β-conversion electron coincidences. Recently, using large Ge detector arrays (Gammasphere, Eurogam), many new transitions have been added to the known level schemes, and several other new nuclei have been identified. In previousl works [1,2], we proposed a method for measuring long half-lives of states by using triple γ coincidence data. In the present work, we propose a new method for measuring short half-lives of the order of ns. In this method, triple γ coincidence spectra in which all three transitions are prompt are compared with the triple γ coincidence spectra in which one of the three transitions is delayed (see Fig. 1 and Table I). Table II shows that the normalized triple γ coincidence counts of two prompt cascades with the similar transition energies are similar. Also, it is observed that the real triple γ coincidence counts or $N1$ values in the prompt cascades vary systematically with the width of the coincidence time window t_w and the three transition energies (see Tables II and III; Figs. 2 and 3). The normalized triple γ coincidence counts or $N1$ values in the prompt cascade increase systematically, not randomly, even at the smaller time windows of 4, 8, and 16 ns. The only difference between the delayed and prompt cascades is that the delayed cascade has one state with a longer half-life. Therefore, the triple γ coincidence counts of a delayed cascade, corrected by normalization factors extracted from the prompt cascade, determine a decay constant λ and half-life by being fitted to the equation $N = C\,(1 - e^{-\lambda t_w})$. Here, t_w is the coincidence time window and C is a constant which is a measure of the coincidence counts at large time windows.

In this method, all of the complicated timing factors, except for the half-life effect in the triple γ coincidence counts of the delayed cascade, are reasonably corrected by the normalization factors obtained from a prompt cascade. Using this techique, we measured the short half-lives of several states in ^{100,104}Zr, ^{106}Mo, and ^{148}Ce. Among the known medium to heavy nuclei, two regions of large deformation have been observed. The nuclei around ^{78}Sr with $Z = 38$ and $N = 40$ [4] and ^{102}Sr with $Z = 38$ and $N = 64$ [5] are known to have large deformation for the 2^+ state. Therefore, it is interesting to determine the deformation for ^{104}Zr with $N = 64$. From the 2^+ state half-life, the quadrupole deformation β_2 is found to be large in ^{104}Zr. We also remeasured the half-lives of states in ^{95,97}Sr and ^{97}Zr in order to prove that the technique works well and to remove existing discrepancies in the previous measurements. The half-life of the first excited state of ^{104}Zr was, for the first time, measured by using the present technique. In the present spontaneous-fissioning work, the centroid shift techniques measuring time difference spectra between two transitions were not used because background in the γ-γ matrix was too high.

TABLE I. Energies of isomeric states E_{IS}, delayed cascades, and corresponding prompt cascades used in simulation. Average numbers of $N1$ values obtained from two prompt cascades are used for ^{97}Sr. d stands for double-gated transitions.

Nuclei	E_{IS}	Delayed cascade	Prompt cascade
^{97}Sr	829.8	522.0^d-205.6-239.6^d	211.7^d-232.3-631.7^d(^{113}Rh)
	307.8	167.0^d-140.8-522.0^d	129.0^d-314.4-157.2^d(^{105}Tc)
			146.0^d-171.9-454.3^d(^{103}Zr)
^{97}Zr	1264.9	1103.4^d-161.5-594.3^d	1090.2^d-578.5-159.5^d(^{102}Zr)
^{95}Sr	556.0	204.0-682.4^d-427.1^d	211.7^d-472.9-635.6^d(^{113}Rh)
^{100}Zr	2259.8	845.1^d-219.5-275.6^d	916.4^d-215.6-298.7^d(^{146}Ba)
^{104}Zr	140.3	140.3^d-312.5-473.3^d	144.3^d-363.1-547.0^d(^{103}Mo)
^{106}Mo	171.8	171.8^d-350.8-545.4^d	172.7^d-374.8-541.6^d(^{109}Ru)
^{148}Ce	158.5	158.5^d-294.9-386.2^d	292.8^d-160.1-415.3^d(^{107}Tc)

II. EXPERIMENTAL TECHNIQUES AND TIME-GATED TRIPLE γ COINCIDENCE METHOD

The γ-γ-γ coincidence measurements were done at LBNL [1,2] with the Gammasphere facility with 72 Ge detectors and a spontaneously fissioning ^{252}Cf source of strength $\sim$28 μCi. The events in the Gammasphere create a time marker with a time-to-digital converter (TDC) for each Ge detector. Several three-dimensional γ-γ-γ coincidence cubes with different coincidence time windows of t_w = 4, 8, 16, 20, 28, 48, 72, 100, 300, and 500 ns between any two Ge detectors [1,2] were built for the three- and higher-fold data using the RADWARE programs [6]. The μs clock registers are latched at the main trigger time. The time-to-amplitude converter in the Gammasphere was started at the main trigger time and stopped at the next μs clock tick. In the time spectra, the time calibration is 4 ns per channel. The measured full width at half maximum (FWHM) of the Ge detector time distribution is approximately 8 ns. The random events in the TDC time difference spectra in a coincidence experiment are dispersed over the entire range of ADC channels. The peak-to-background ratios are about 5 for a typical single gate and 20 for a double gate. Of course, these ratios depend on the relative intensities of the γ transitions in the level scheme. Since the random events in the triple γ coincidence spectra are greatly reduced, we have not considered the random events in this paper.

The prompt cascade is one in which the half-lives of the states considered are shorter than 500 ps. For example, half-lives of 300 and 500 ps and 1 ns will make a difference in the total counts of 0.0097%, 0.39%, and 6.25%, respectively, at a 4 ns time window. For the present work, consider two cascades, as shown in Fig. 1, in which the energies of the transitions are similar in each cascade. In the delayed cascade, one state has a half-life greater than 1 ns, which we would like to measure.

A time-gated cube consists of all triple-coincidence events for which the time differences between any two of the Ge detectors are less than the specified coincidence time window t_w. Transition energy dependent effects such as risetime walks, time jitters, amplitude walks, and possible timing fluctuations of Ge detectors become important for lower energy transitions and for shorter coincidence time windows. Already, a time-gated triple γ coincidence method using a delayed cascade consisting of four γ transitions was used to extract longer half-lives of several states [1,2]. In Table II, the relative triple coincidence counts are compared for two sets of transitions in ^{152,154}Nd. Both sets have very similar transition energies. It is observed that these relative coincidence counts are consistent within errors. The present method is to compare the delayed and prompt cascades consisting of three γ transitions with very similar energies to extract half-lives. The half-lives of several states in ^{95,97}Sr, ^{97,100,104}Zr, ^{106}Mo, and ^{148}Ce, which are shown in Table I, have been measured.

TABLE II. Relative triple γ coincidence counts, $N(\gamma; t_w)/N(\gamma; t_w = 500)$, in four prompt cascades. d stands for double-gated transitions.

Time window ns	^{152}Nd 247.4^d-322.2-389.9^d	^{154}Nd 248.6^d-328.2-400.7^d	^{152}Nd 164.2^d-247.4-322.2^d	^{154}Nd 162.8^d-248.6-328.2^d
4	0.174(2)	0.173(2)	0.122(2)	0.123(2)
8	0.357(3)	0.352(4)	0.267(2)	0.274(3)
16	0.687(5)	0.680(6)	0.583(4)	0.589(5)
20	0.767(5)	0.763(7)	0.681(4)	0.687(5)
28	0.848(6)	0.844(7)	0.795(5)	0.798(6)
48	0.781(5)	0.773(7)	0.756(5)	0.754(6)
72	0.929(6)	0.925(8)	0.912(5)	0.907(7)
100	1.212(8)	1.219(10)	1.206(7)	1.198(9)
300	0.885(6)	0.882(8)	0.881(5)	0.878(7)
500	1.00(1)	1.00(1)	1.00(1)	1.00(1)

TABLE III. Normalization factors $N1 = N(\gamma; t_w = 500)/N(\gamma; t_w)$ of several prompt cascades used in the present work. Note that the $N1$ values increase systematically with the decreasing time window and with decreasing transition energies even at smaller time windows of 4, 8, and 16 ns. In all prompt cascades, half-lives of states are of the order of a few hundred ps [3].

Time window ns	^{113}Rh 211.7-472.9-635.6	^{105}Tc 129.0-314.4-157.2	^{103}Zr 146.0-171.9-454.3	^{113}Rh 211.7-232.3-631.7	^{146}Ba 916.4-215.6-298.7
4	5.61(14)	10.07(30)	9.95(49)	7.69(24)	5.62(46)
8	2.70(5)	4.59(10)	4.49(17)	3.48(8)	2.69(19)
16	1.47(3)	1.96(3)	1.91(6)	1.61(3)	1.42(9)
20	1.32(2)	1.72(3)	1.58(4)	1.40(3)	1.27(8)
28	1.19(2)	1.40(2)	1.39(4)	1.24(3)	1.17(7)
48	1.31(2)	1.38(2)	1.32(4)	1.31(3)	1.21(7)
72	1.10(2)	1.14(1)	1.12(3)	1.10(2)	1.07(6)
100	0.83(1)	0.86(1)	0.84(2)	0.82(2)	0.83(5)
300	1.14(2)	1.13(1)	1.14(3)	1.14(2)	1.14(7)
500	1.00(2)	1.00(1)	1.00(3)	1.00(2)	1.00(6)
^{102}Zr	^{103}Mo	^{107}Tc	^{107}Tc	^{109}Ru	
1090.2-578.5-159.5	144.3-363.1-547.0	292.8-160.1-415.3	172.6-329.1-482.7	172.7-374.8-541.6	
6.12(14)	7.28(14)	7.40(25)	6.48(13)	6.24(13)	
3.15(5)	3.57(5)	3.67(10)	3.22(5)	2.94(5)	
1.61(2)	1.70(2)	1.74(4)	1.58(2)	1.60(2)	
1.40(2)	1.45(1)	1.48(3)	1.38(2)	1.37(2)	
1.24(2)	1.25(1)	1.27(3)	1.22(2)	1.22(2)	
1.32(2)	1.30(1)	1.34(3)	1.29(2)	1.29(2)	
1.10(1)	1.09(1)	1.13(2)	1.10(1)	1.09(1)	
0.82(1)	0.83(1)	0.84(2)	0.84(1)	0.83(1)	
1.14(2)	1.12(1)	1.15(2)	1.15(2)	1.13(2)	
1.00(1)	1.00(1)	1.00(2)	1.00(1)	1.00(1)	
^{152}Nd	^{154}Nd	^{152}Nd	^{154}Nd		
247.4[d]-322.2–389.9[d]	248.6[d]-328.2–400.7[d]	164.2[d]-247.4–322.2[d]	162.8[d]-248.6–328.2[d]		
5.75(6)	5.79(8)	8.18(8)	8.12(11)		
2.80(2)	2.84(3)	3.75(3)	3.66(4)		
1.46(1)	1.47(1)	1.72(1)	1.70(1)		
1.30(1)	1.31(1)	1.47(1)	1.46(1)		
1.18(1)	1.18(1)	1.26(1)	1.25(1)		
1.28(1)	1.29(1)	1.32(1)	1.33(1)		
1.08(1)	1.08(1)	1.10(1)	1.10(1)		
0.83(1)	0.82(1)	0.83(1)	0.83(1)		
1.13(1)	1.13(1)	1.14(1)	1.14(1)		
1.00(1)	1.00(1)	1.00(1)	1.00(1)		

The factors that contribute to the shape and width of the timing spectra are rise time walks, time jitters, and amplitude walks. The dominant factor which contributes to the shape and width of the timing spectra is the time resolution of Ge detectors. These factors become large for (a) low-energy γ transitions and (b) very small time windows. Additional factors that contribute to the width and shape are (a) variations in the position of the time marker from different Ge detectors (possible timing fluctuations) and (b) half-lives of the states. All these factors depend on the energies of the transitions in the cascade. Our previous [1,2] and current data show that the factors for higher energy transitions and for larger time windows (>100 ns) can be neglected in extracting their half-lives. Also, the total counts of each time-gated cube may be different because the total events processed for each time window may be different. In the prompt cascade, if the factors discussed above are negligible, the prompt spectrum will resemble a δ function. The main contribution to the Gaussian shape of the prompt spectrum is due to the time resolution of Ge detectors; the time walk usually makes this Gaussian shape asymmetric. However, as shown in Table II and in Fig. 2, one has to correct the prompt spectrum for these factors. Hence, one gets the correction factors for the prompt cascade by comparing the coincidence counts at window t_w to that at $t_w = 500$ ns, that is, $N1 = N(\gamma; t_w = 500)/N(\gamma; t_w)$. These correction factors are common to both delayed and prompt cascades. The deviation of these numbers from unity is a measure of the effects discussed above. In Fig. 2, there are relatively more counts in the 48 ns time window and relatively fewer counts in the 100 ns time window for all of prompt cascades. Those effects are seen for all of the prompt cascades in Table II. In Fig. 3, the values normalized to the

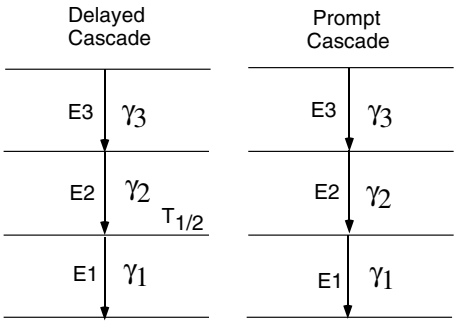

FIG. 1. Delayed and prompt cascades. Double gates are set on γ_3 and γ_1 to get the triple coincident counts of γ_2. The state with the half-life can be either the second or third one in the delayed cascade.

prompt cascade consisting of 1750, 1106.7, and 915.0 keV transitions in ^{96}Zr are drawn in order to show the transition energy dependent effects. Note that the deviation of $N1$ from a smooth curve by decreasing at 48 ns and increasing at 100 ns does not appear in Fig. 3. This indicates that the relatively more counts in the 48 ns time window, the relatively fewer counts in the 100 ns time window, and somewhat more in the 300 ns time window in Fig. 2 and Table III are caused mainly by the total number of events processed for each time window but not by the transition energy dependent timing effects. Differences in the total number of events arise because in scanning the data tapes, a part of some tapes cannot be scanned due to bad blocks. Also, Table III shows several $N1$ values which we used to extract the half-lives in the present work.

Now, when one compares prompt and delayed cascades in which each of the three transition energies in each cascade

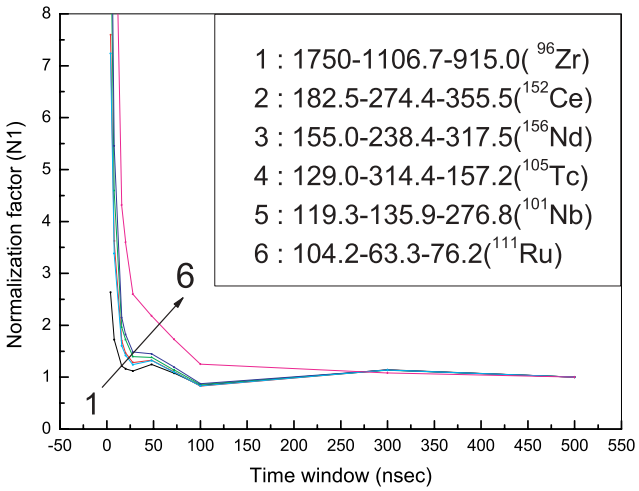

FIG. 2. (Color online) $N1$ normalization factors obtained from several prompt cascades normalized to the coincident counts at the time window of 500 ns. More counts at the 48 ns time window and fewer counts at the 100 ns time window observed for all the prompt cascades are caused mainly by the time-window-dependent total count difference of each time-gated cube. Half-lives of the states in these prompt cascades (except the low-energy cascade in ^{111}Ru) are less than a few hundred ps [3]. The ^{111}Ru cascade with half-lives of 14 ns and 5 ns [3] for the states within the cascade is included to show that the timing effects are much larger for low-energy transitions.

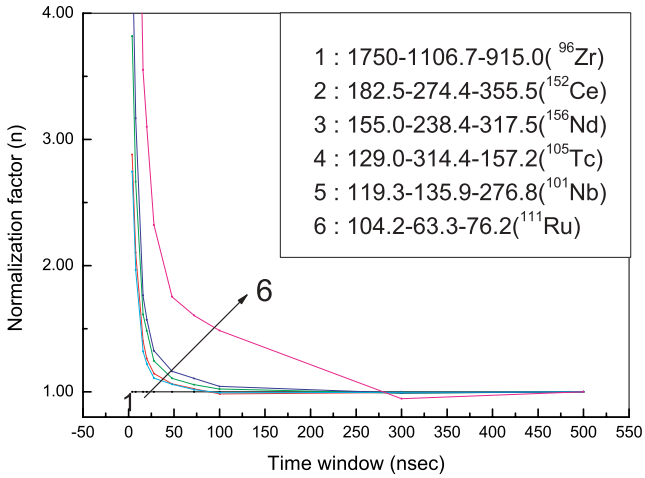

FIG. 3. (Color online) Normalization factors n showing the timing effects dependent on the triple transition energies of several prompt cascades. These are normalized to the prompt cascade 1750.0-1106.7-915.0 in ^{96}Zr. Note that the more counts at 48 ns and the fewer counts at 100 ns seen in the $N1$ plot (Fig. 2) are removed in this n plot.

are very similar, the only difference between the delayed and prompt cascades is that the delayed cascade has a state with a long half-life, whereas the prompt cascade does not. All other factors except the half-life effect are common to both delayed and prompt cascades. Therefore, the triple coincidence counts of each time-gated cube in the delayed cascade should be multiplied by $N1$ as a correction factor. This is because the triple γ coincidence counts of the delayed and prompt cascades were recorded under the same experimental conditions. The correction procedure using the $N1$ value as correction factor is only approximately valid, to about 10% and at the most 20%. Then, the corrected counts in the delayed cascade should follow the equation with the decay constant λ. More details are explained in the following paragraphs.

A Monte Carlo simulation was carried out to find the systematic errors by using the convolution between time decay distribution and detector time resolution. The FWHM for a single Ge detector in the Gammasphere is 8 ns for the time distribution. In this simulation, we used the time windows of 4, 8, 16, 20, 28, 48, 72, 100, 300, and 500 ns for the present data analysis. In Table IV, we show the results of our simulation. The first column shows the decay time of the state used, and the second column shows the simulated values. The error in the third column is the % error between these two values. From the simulation results, the systematic errors of 10% were added to our measured half-lives, except the half-life of 0.9 ns in ^{148}Ce, to which the systematic error of 20% was added.

Consider a downward cascade consisting of γ_3-γ_2-γ_1 transitions, where γ_1 is the outgoing transition from a state with a long half-life and γ_2 is the incoming transition into the same state. The other state between γ_3 and γ_2 in this cascade is assumed to have a very short (prompt) half-life. Double gates are set on γ_3 and γ_1 and the intensity of $N(\gamma_2)$ is measured in each spectra. The coincidence time window t_w of interest is set for these triple γ coincidences. The half-lives of top

TABLE IV. Monte Carlo simulation by using the convolution between time decay distribution and detector time resolution. FWHM for the Ge detector is 8 ns which is used for simulation. Decay time T_d is $1/\lambda$, and $T_{1/2}$ is $\ln 2/\lambda$.

T_d (ns)	Simulated T_d (ns)	Error (%)	$T_{1/2}$(ns)
150	163	7.9	104.0
100	108	7.4	69.3
40	44	9.1	27.7
10	11	9.1	6.9
6	6.6	9.1	4.2
2	2.2	9.1	1.4
1	1.3	23	0.69

and bottom states do not make any contribution to these triple coincidences.

Therefore, $N(\gamma_2)$ intensity observed from the state with the decay constant λ of interest should follow the equation $N(\gamma_2) = C(1 - e^{-\lambda t_w})$, where t_w is the coincidence time window. $N(\gamma_2)$ does not have to be corrected for the constant effects such as the detector efficiency and internal conversion electron coefficient, because these can be included in the constant C, where these correction factors affect each time window the same. But $N(\gamma_2)$ of the delayed cascade has to be multiplied by a normalization factor ($N1$). After multiplying the coincident counts of $N(\gamma_2)$ with $N1$, we plotted the normalized numbers of counts $N = N(\gamma_2)N1$ vs coincidence time window t_w to extract the half-lives.

In Fig. 2, a prompt cascade consisting of the 1750.0, 1106.7, and 915.0 keV transitions in ^{96}Zr shows a steep increase at the time window between 4 and 8 ns arising mainly because the correction factor increases with decreasing time window and total count difference between the different time-gated cubes. In order to show the triple energy dependent timing effects, we plotted the counts n of several prompt cascades normalized to the prompt cascade consisting of 1750.0, 1106.7, and 915.0 keV transitions in ^{96}Zr (Fig. 3). Here, $n = N1/N1(^{96}\mathrm{Zr})$. In Fig. 2, the $N1$ values of the prompt cascade with lower transition energies increase more than those with the higher transition energies. In the case of the prompt cascade consisting of 104.2, 63.3, and 76.2 keV, transitions in ^{111}Ru, the timing effects are large even at the time window of 200 ns, as shown in Fig. 3. However, the other five cascades in Figs. 2 and 3 show smaller timing effects at the time window of $\leqslant$100 ns. If all three transition energies are larger than 200 keV, the timing effects are small ($<$15%) even at the time window of $\approx$20 ns, as shown in Fig. 3. Therefore, in order to analyze the coincidence data at lower transition energies and at time windows shorter than 100 ns, the timing effects have to be taken into account.

In the present work, these timing effects for the delayed cascades of interest are corrected by using the corresponding prompt cascades as shown in Table I. Then, the normalization factors $N1$ in Table III are determined from the corresponding prompt cascades with very similar transition energies in the last column of Table I. $N(\gamma_2)$ is replaced with $N(\gamma_2)N1$ in the equation to extract the half-life. Ten spectra with the time windows of 4, 8, 16, 20, 28, 48, 72, 100, 300, and 500 ns are used in the analysis.

The normalization procedure described above to eliminate problems of time walks, time jitters, etc., was confirmed to work by the fact that (1) our measured half-lives agree with previous measurements in several cases to be discussed with half-lives of 1 to 265 ns and with delayed transition energies from 152 to 1265 keV and (2) we observed no half-lives $T_{1/2} \ll 1$ ns (see Fig. 5) in several known prompt cascades.

III. RESULTS AND DISCUSSION

Initially this method was applied to the prompt cascade consisting of three transitions (248.6-328.2-400.7 keV) in ^{154}Nd in which the second and third states have half-lives of the order of a few ps. The normalization factors $N1$ are obtained from the prompt cascade consisting of 247.4-322.2-389.9 keV transitions in ^{152}Nd, as shown in Table II. Eight time-gated coincidence spectra with double gates on 247.4 and 389.9 keV in ^{152}Nd and 248.6 and 400.7 keV in ^{154}Nd are shown in Fig. 4. The normalized coincidence counts N of the 328.2 keV

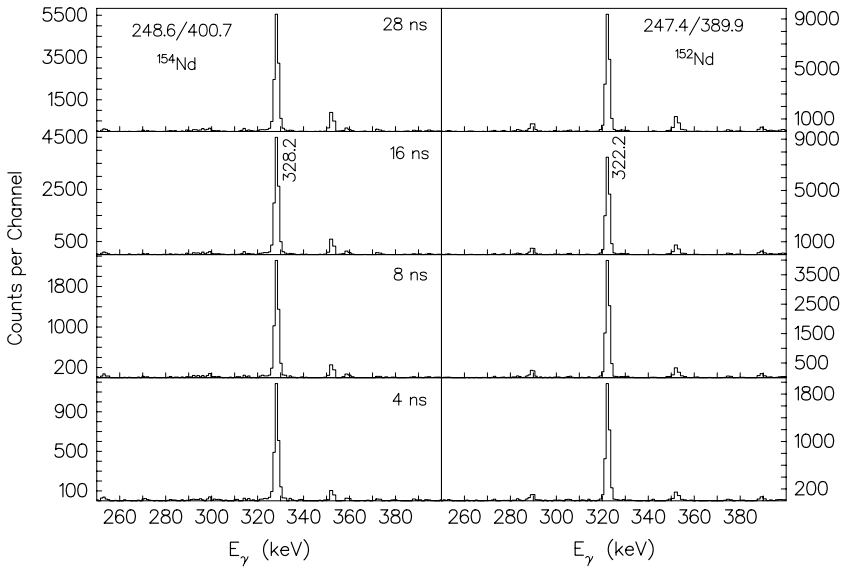

FIG. 4. Time-gated coincident spectra with double gates on 248.6 and 400.7 keV transitions for the prompt cascade consisting of 248.6 ($6^+ \rightarrow 4^+$), 328.2 ($8^+ \rightarrow 6^+$), and 400.7 ($10^+ \rightarrow 8^+$) keV transitions in ^{154}Nd and on 247.4 and 389.9 keV transitions for the prompt cascade of 247.4 ($6^+ \rightarrow 4^+$), 322.2 ($8^+ \rightarrow 6^+$), and 389.9 ($10^+ \rightarrow 8^+$) keV transitions in ^{152}Nd.

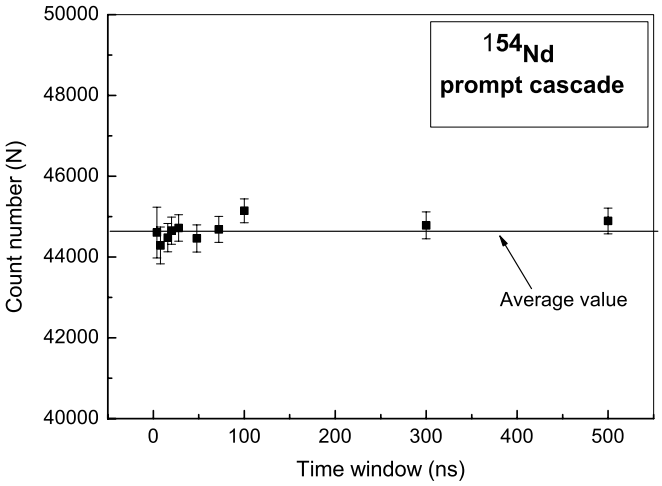

FIG. 5. Normalized count N vs coincident time window for prompt cascade 248.6-328.2-400.7 keV in ^{154}Nd. N values are essentially constant as expected for a prompt cascade with half-life of the order of ps. $N1$ values obtained from the prompt cascade 247.4-322.2-389.9 keV in ^{152}Nd are used.

transition are plotted in Fig. 5. The experimental data in Fig. 5 are almost constant, indicating that this cascade in ^{154}Nd is really a prompt cascade as expected.

For a state with half-life of 2 ns, the N values at 4, 8, and 16 ns time windows are 25%, 6.25%, and 0.39% smaller than the C value, respectively, as calculated from $[(C - N)/C] \times 100\%$. The count difference of 25% at the time window of 4 ns can be measured reasonably well if the coincidence peak

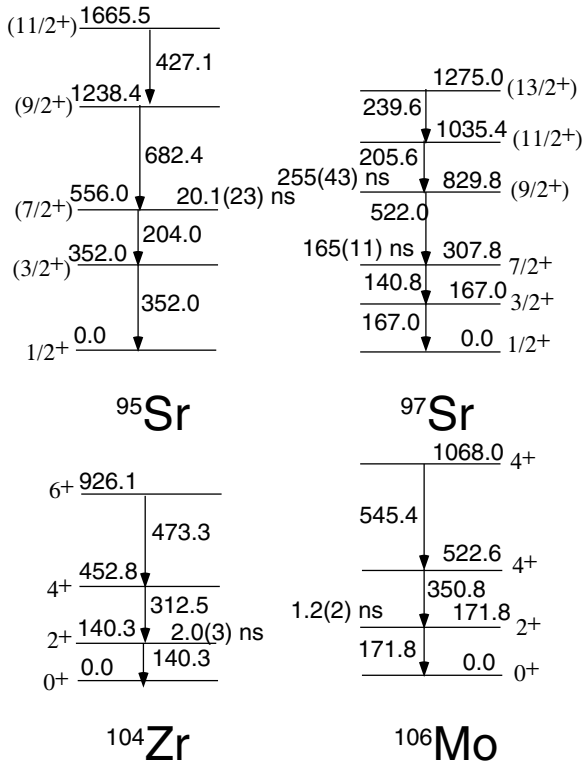

FIG. 6. Partial level schemes of ^{95,97}Sr, ^{104}Zr, and ^{106}Mo.

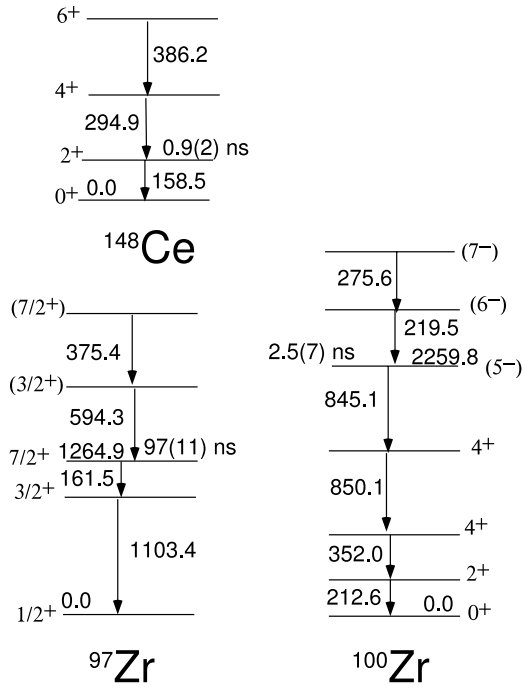

FIG. 7. Partial level schemes of ^{97,100}Zr and ^{148}Ce.

is strong and has negligible background under the peak. This means that in the best cases, with very strong coincidence peaks and negligible background counts, a half-life of ≈1 ns can be measured. Therefore, in the present work, several cases, including states with short half-lives, are shown in Figs. 6 and 7. In Figs. 6 and 7, only partial level schemes of these isotopes are shown.

For ^{97}Sr, the half-lives of 167.0, 307.8, and 829.8 keV states have been measured [3,7,8,9] to be 0.22(4), 170(10), and 255(10) ns, respectively, from β^- decay work of ^{97}Rb. Also, the combined half-life of the 307.8 and 829.8 keV states was measured to be 0.43(3) μs from the thermal n-induced fission of ^{241}Pu [10]. For comparison, the half-life of the 307.8 keV state was remeasured using the delayed cascade consisting of 167.0-140.8-522.0 keV transitions. The average $N1$ values from two prompt cascades 129.0-314.4-157.2 (^{105}Tc) and 146.0-171.9-454.3 (^{103}Zr), as shown in Table III, were used. As an example, time-gated coincidence spectra with double gates on the 167.0 and 522.0 keV in ^{97}Sr are shown in Fig. 8 for $t_w = 4$, 8, and 16 ns. The normalized coincidence counts of the 140.8 keV transition are plotted in Fig. 9. A half-life of 165(9) ns for the 307.8 keV state is obtained by fitting these data with the formula and is consistent with the previously measured half-life of 170(10) ns [8]. For further comparison, the half-life of the 829.8 keV state was measured by using the delayed cascade consisting of 522.0-205.6-239.6 keV transitions and $N1$ values from the prompt cascade consisting of 211.7-232.3-631.7 transitions (^{113}Rh). Time-gated coincidence spectra with double gates on the 522.0 and 239.6 keV transitions in ^{97}Sr are shown in Fig. 8. The normalized coincidence counts of the 205.6 keV transition are plotted in Fig. 9. By fitting these data to the equation, a half-life of 255(30) ns for the 829.8 keV state is extracted.

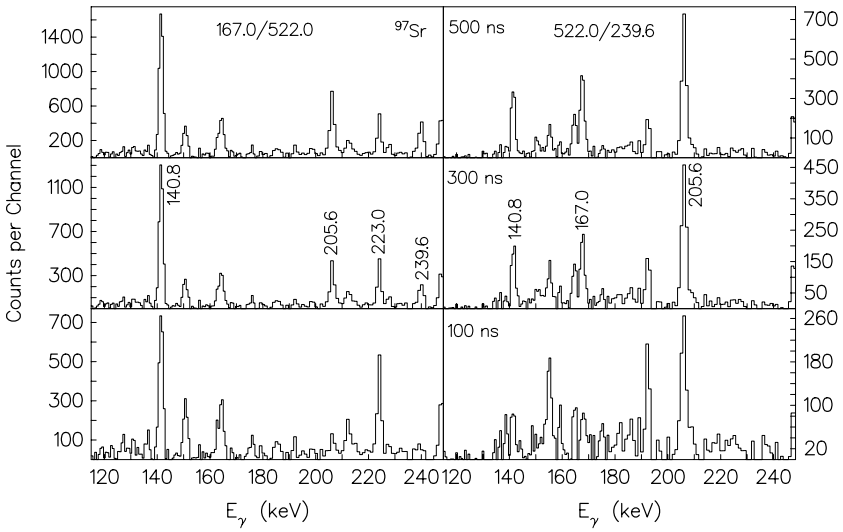

FIG. 8. Time-gated coincident spectra with double-gates on 167.0 and 522.0 keV transitions for the delayed cascade 167.0-140.8-522.0 keV and on 522.0 and 239.6 keV transitions for the delayed cascade 522.0-205.6-239.6 keV in ^{97}Sr. Marked peaks belong to ^{97}Sr.

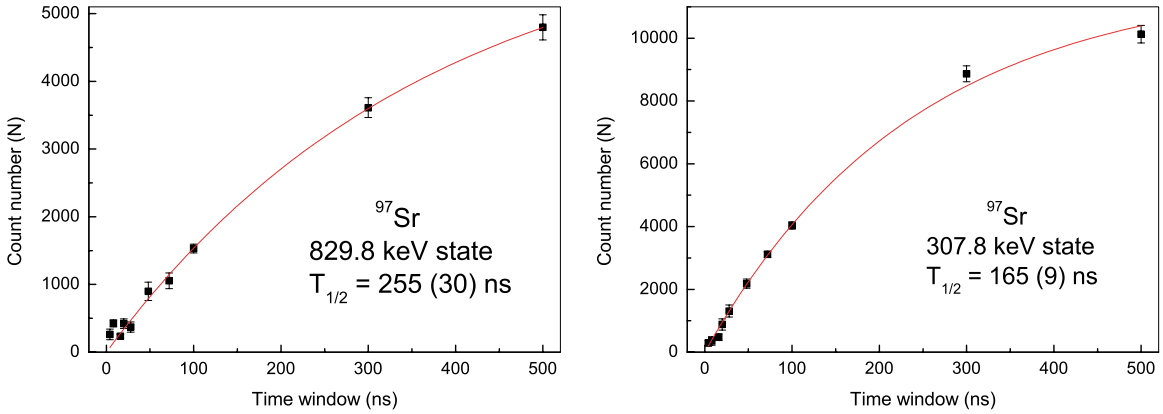

FIG. 9. (Color online) Normalized count N vs coincident time window in ^{97}Sr.

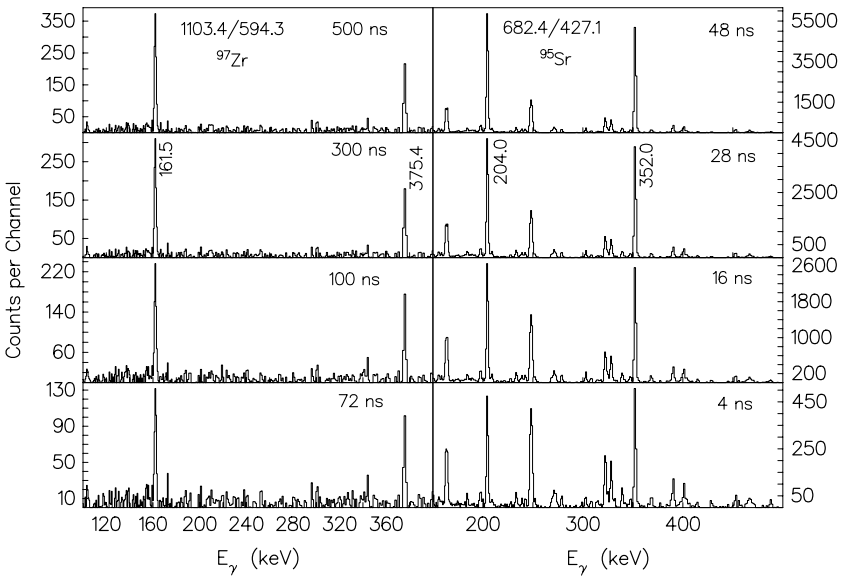

FIG. 10. Time-gated coincident spectra with double gates on 1103.4 and 594.3 keV transitions for the delayed cascade 1103.4 > 161.5-594.3 keV in ^{97}Zr, and on 682.4, and 427.1 keV transitions for the delayed cascade 204.0-682.4 > 427.1 keV in ^{95}Sr.

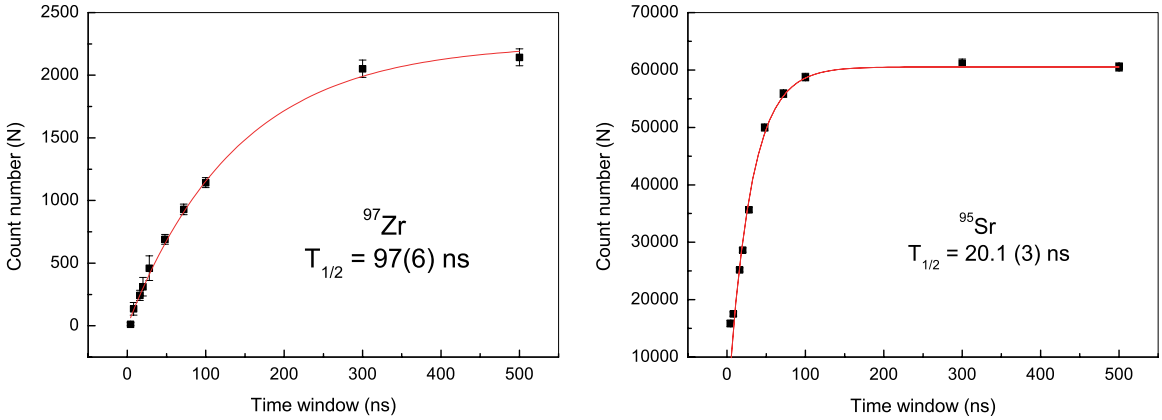

FIG. 11. (Color online) Normalized count N vs coincident time window in ^{97}Zr and ^{95}Sr. Half-lives are for the 1264.9 keV state in ^{97}Zr and 556.0 keV state in ^{95}Sr.

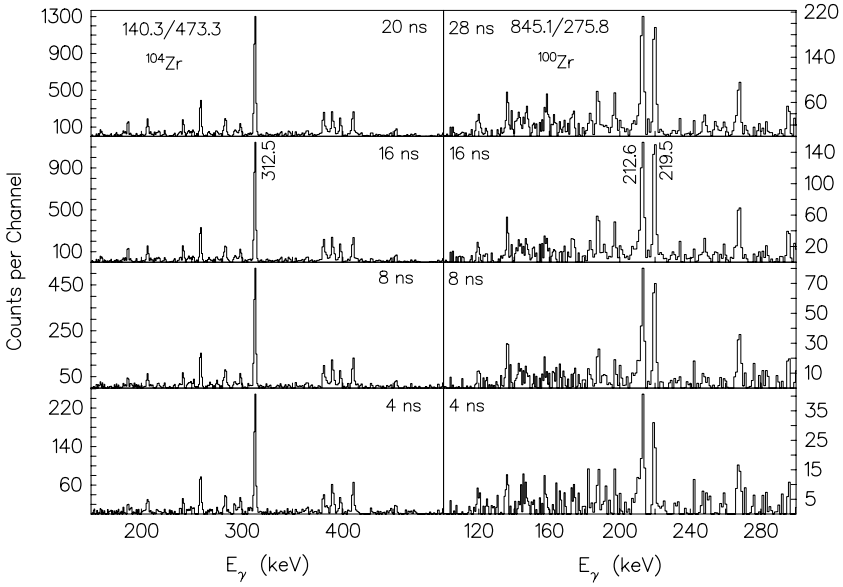

FIG. 12. Time-gated coincident spectra with double gates on 845.1 and 275.6 keV transitions for the delayed cascade 845.1-219.5-275.6 in ^{100}Zr, and on 140.3 and 473.3 keV transitions for the delayed cascade 140.3-312.5-473.3 in ^{104}Zr.

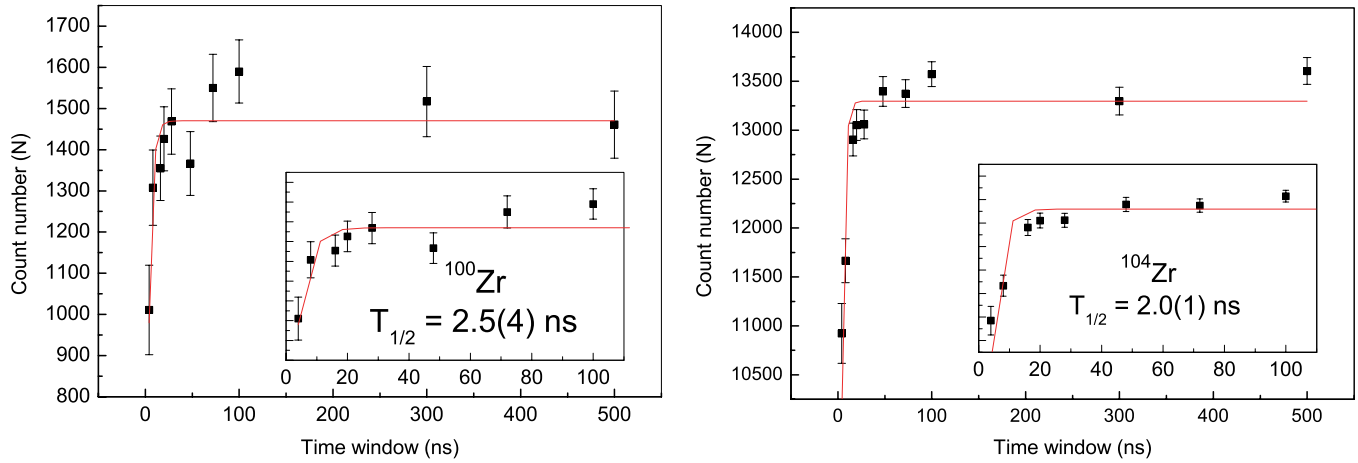

FIG. 13. (Color online) Normalized count N vs coincident time window in ^{100}Zr and ^{104}Zr. Half-lives are for the 2259.8 state in ^{100}Zr and 140.3 keV state in ^{104}Zr.

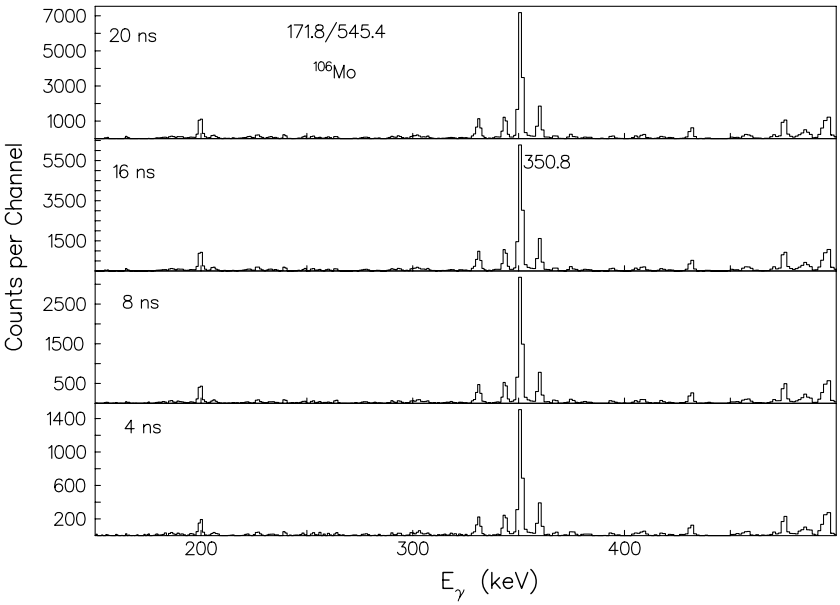

FIG. 14. Time-gated coincident spectra with double gates on 171.8 and 545.4 keV transitions for the delayed cascade 171.8-350.8-545.4 in ^{106}Mo.

The present value is consistent with the half-lives [1,9] previously obtained.

A weighted average half-life of the 1264.9 keV state in ^{97}Zr is 103(3) ns [3,11,12]. For further comparison, the half-life that was measured with the delayed cascade consisting of 1103.4-161.5-594.3 keV transitions and $N1$ values from the prompt cascade consisting of 1090.2-578.5-159.5 keV transitions (^{102}Zr) are shown in Tables I and III. Four time-gated coincidence spectra with double gates on 1103.4 and 594.3 keV transitions in ^{97}Zr are shown in Fig. 10. The normalized coincidence counts of the 161.5 keV transition are plotted in Fig. 11. A half-life of 97(6) ns for the 1264.9 keV state is obtained by fitting these data to the equation and is consistent with the earlier measurements.

For ^{95}Sr, in the Enhanced Nuclear Structure Data File (ENSDF) [3], a half-life of 21.7(5) ns is reported for the 556.0 keV state from a weighted average of several measurements [13,14,15]. In the present work, the half-life of the 556.0 keV state is measured from the delayed cascades consisting of 204.0-682.4-427.1 keV transitions as shown in Table I. The corresponding prompt cascades and their $N1$ factors used in the present work are shown in Table III. The time-gated coincidence spectra with double gates on 682.4 and 427.1 keV transitions in ^{95}Sr are shown in Fig. 10. The triple γ coincidence counts obtained from these spectra fitted to the equation are shown in Fig. 11. The obtained half-life of the 556.0 keV state is 20.1(3) ns. This half-life is consistent with the previously measured half-lives [3], as shown in Table IV.

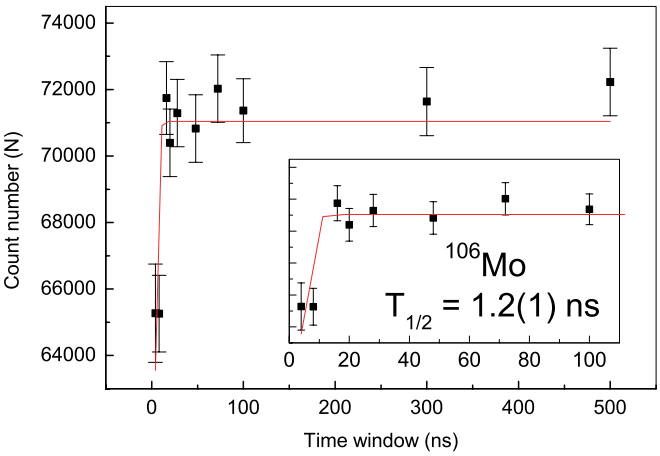

FIG. 15. (Color online) Normalized count N vs coincident time window in ^{106}Mo. Half-life is for 171.8 keV state in ^{106}Mo.

The half-life of the 2259.8 keV state in ^{100}Zr has never been measured. To measure this half-life, the delayed cascade of 845.1-219.5-275.6 keV transitions was used with the $N1$ values from the prompt cascade of 916.4-215.6-298.7 keV transitions (^{146}Ba), as shown in Tables I and III. Time-gated coincidence spectra with double gates on 845.1 and 275.6 keV in ^{100}Zr are shown in Fig. 12. The normalized coincidence counts of the 219.5 keV transition are plotted in Fig. 13. A half-life of 2.5(4) ns for the 2259.8 keV state is obtained by fitting these data to the equation.

The half-life of the 2^+ state in ^{104}Zr is determined for the first time in the present work. In Table I, the delayed cascade in ^{104}Zr and the prompt cascade in ^{103}Mo are tabulated. In Fig. 12, the coincidence spectra double-gated on the 140.3 and 473.3 keV transitions are shown. A purely statistical fit gives the half-life of the 2^+ state in ^{104}Zr as 2.0(1) ns, (Fig. 13).

For ^{106}Mo, previously measured half-lives of the 171.8 keV state are 1.25(3) [16], 0.372(54) [17], 0.75(15) [18], and 1.34(54) [19] ns. In the present work, we tried to confirm these short half-life values. In Table I, the delayed cascade in ^{106}Mo and the two prompt cascades in ^{107}Tc and ^{109}Ru are tabulated. In Fig. 14, the coincidence spectra double-gated on the 171.8 and 545.4 keV transitions are shown. An average of two $N1$ values obtained in the two prompt cascades are used here to get N in Fig. 15. The half-life obtained for the 2^+ state in ^{106}Mo is 1.2(1) ns, which is consistent with three of the previous values.

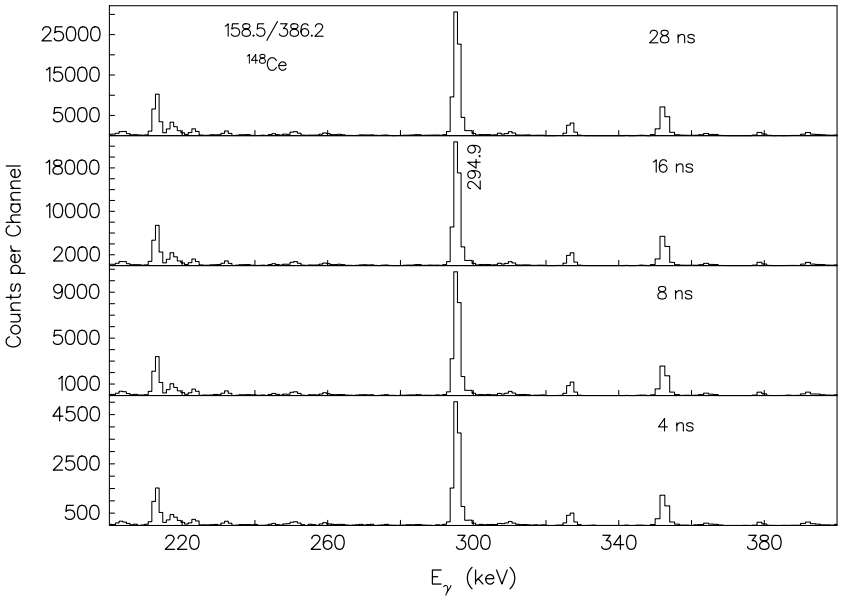

FIG. 16. Time-gated coincident spectra with double gates on 158.5 and 386.2 keV transitions for the delayed cascade consisting of 158.5, 294.9 and 386.2 keV transitions in ^{148}Ce.

For ^{148}Ce, the half-life of the 158.5 keV state was reported to be 0.95(8) [20], 1.06(8) [16], 1.3(2) [21], and 1.04(7) [22] ns from the spontaneous fissioning of ^{252}Cf. The weighted average value of the two half-lives of 0.95(8) and 1.06(8) ns is reported in ENSDF [3]. To measure the half-life of the 158.5 keV state, the delayed cascade of 158.5-294.9-386.2 keV transitions is used with $N1$ values from the prompt cascade of 292.8-160.1-415.3 keV transitions (^{107}Tc), as shown in Tables I and III. Time-gated coincidence spectra with double gates on 158.5 and 386.2 keV transitions in ^{148}Ce are shown in Fig. 16. The normalized coincidence counts N of the 294.9 keV transition are shown in Fig. 17. A half-life of 0.9(1) ns for the 158.5 keV state is obtained by fitting these data with the equation. The present half-life is consistent with the previously reported values. The known half-life is so short in this case that essentially only the shortest time window point in our different time windows should be well below the flat region, and this is what is found.

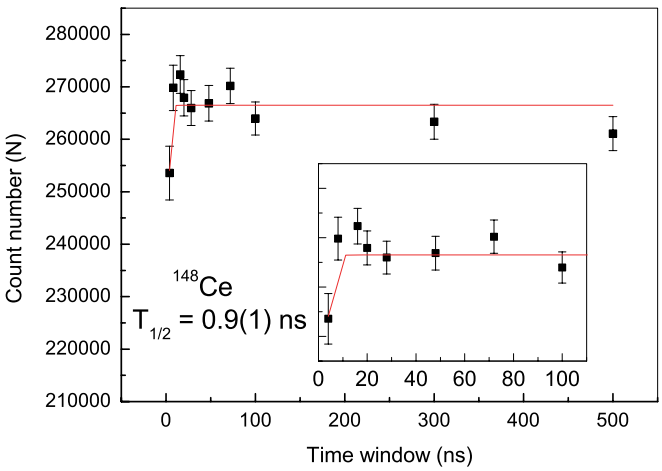

FIG. 17. (Color online) Normalized count N vs coincident time window in ^{148}Ce. Half-life is for 158.5 keV state in ^{148}Ce.

The extracted $B(E2; 2^+ \rightarrow 0^+)(e^2\,b^2)$ values and quadrupole deformations β_2 for ^{102,104}Zr, ^{106}Mo, and ^{148}Ce are shown in Table V. According to our data, ^{104}Zr with $\beta_2 = 0.47(7)$ has a larger deformation than that of ^{102}Zr with $\beta_2 = 0.42(16)$. In Fig. 18, the quadrupole deformation vs proton number Z is plotted. Present quadrupole deformation values of ^{104}Zr and ^{106}Mo are added in Fig. 18. Among medium and heavy nuclei, ^{104}Zr is the most deformed except for ^{102}Sr [4]. Therefore, two regions of large deformation in the medium and heavy even-even nuclei are observed at ^{78}Sr, and ^{102}Sr-^{104}Zr. Intruder orbitals of $1g_{9/2}9/2[404]$ and $2f_{7/2}1/2[541]$ around $N = 64$ and $2d_{5/2}1/2[431]$ around $N = 40$ and $Z = 38$ may produce the large deformation in ^{78}Sr, ^{102}Sr, and ^{104}Zr as a result of the reinforcement of the proton and neutron shell gaps at large deformation [27]. Recently, theoretical calculations for the β_2

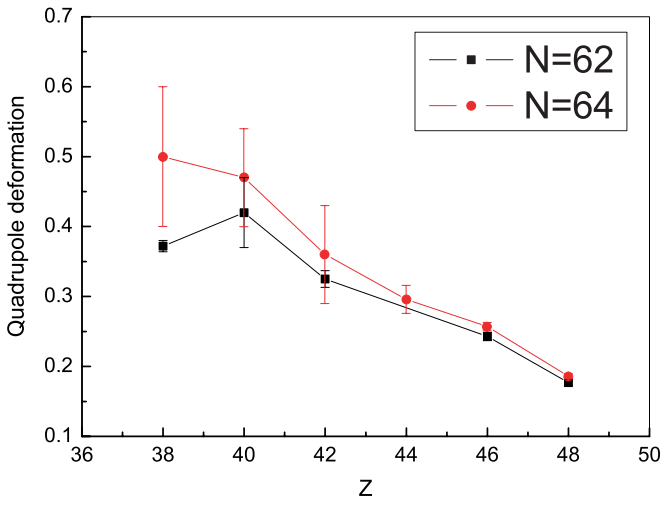

FIG. 18. (Color online) Quadrupole deformation β_2 vs proton number Z. The β_2 value of ^{102}Sr [0.50(10)] is obtained from the previously known half-life of 3.0(12) ns [5]. β_2 values in other nuclei except ^{102}Sr, ^{104}Zr, and ^{106}Mo are obtained from Ref. [4]. β_2 values of ^{104}Zr, and ^{106}Mo are added from the present work.

TABLE V. States (E_{IS}) with half-lives, half-lives $T_{1/2}$ (ns), $B(E2; 2^+ \rightarrow 0^+)(e^2\,b^2)$, and β_2 values. Adopted final values for the half-lives include the systematic errors of 10%, for ^{148}Ce a systematic error of 20% is added.

Nucleus	E_{IS}	$T_{1/2}$	Ref. $T_{1/2}$	ENSDF
^{97}Sr	829.8	255(56)	265(27)[1], 255(10)[9]	255(10)
	307.8	165(25)	170(10)[8]	170(10)
^{97}Zr	1264.9	97(16)	102(3)[11], 104(5)[12]	103(3)
^{95}Sr	556.0	20.1(23)	23.6(24)[1],21.8(11)[14] 24.0(12)[15],20.9(5)[13]	21.7(5)
^{100}Zr	2259.8	2.5(7)		
^{104}Zr	140.3	2.0(3)		
^{106}Mo	171.8	1.2(2)	0.75(15)[18], 1.25(3)[16] 1.34(54)[19], 0.37(5)[17]	1.25(3)
^{148}Ce	158.5	0.9(3)	0.95(8)[20], 1.06(8)[16] 1.3(2)[21], 1.04(7)[22]	1.01(6)
Nucleus	$B(E2)$	β_2	β_2 (theory)	α_{total}
^{104}Zr	0.40(6)	0.47(7)	0.45[23],0.43[24]	0.328[25]
^{106}Mo	0.29(4)	0.36(7)		0.172[26]
^{148}Ce	0.45(12)	0.27(7)		0.411[3]

value of ^{104}Zr were carried out by solving the Hartree-Fock-Bogoliubov (HFB) equations for the mean field and pairing field in coordinate space. Large deformations of 0.45[23] and 0.43[24] were found in the theoretical calculations for ^{104}Zr. These are consistent with our measurements.

IV. SUMMARY

In summary, we report half-lives of several states in neutron-rich nuclei produced in the spontaneous fission of ^{252}Cf by using a novel method of comparing the delayed and prompt cascades consisting of three γ transitions. It is shown that the normalized triple γ coincidence counts of two prompt cascades with similar transition energies are similar. Also, it is observed that the real triple γ coincidence counts in the prompt cascades change systematically along with the change of the coincidence time window and three transition energies. The half-lives of the states in the delayed cascades are approximately determined by using the prompt cascades with similar transition energies to that of delayed cascades. The systematic error is predicted to be typically below 10%.

The half-lives of 2^+ states in ^{104}Zr and ^{106}Mo are measured to be 2.0(3) and 1.2(2) ns, respectively. The obtained $B(E2; 2^+ \rightarrow 0^+)(e^2\,b^2)$ values and quadrupole deformations β_2 are 0.40(6) ($e^2\,b^2$) and 0.47(7) for ^{104}Zr and 0.29(4) ($e^2\,b^2$) and 0.36(7) for ^{106}Mo. Except for ^{102}Sr, ^{104}Zr is the most deformed among the medium and heavy nuclei. This large deformation for ^{104}Zr is in agreement with the HFB calculation [24,25]. If a corresponding prompt cascade can be found along with the delayed cascade in the same experiment, the present method will be applicable for half-life measurements on the ns scale not only in the triple γ coincidence data but also in the γ-γ matrix data.

ACKNOWLEDGMENTS

We acknowledge the help of K. E. Gregorich and A. O. Macchiavelli at LBNL with Gammasphere and the discussions with J. O. Rasmussen at LBNL, D. Radford at ORNL, and H. L. Crowell at Vanderbilt University. The work at Vanderbilt University, LBNL, and Idaho National Laboratory is supported by the U.S. DOE under Grant No. DE-FG05-88ER40407 and Contract Nos. DE-AC03-76SF00098 and DE-AC07-76ID01570, respectively. The work at Tsinghua University is supported by the Major State Basic Research Development Program under Grant No. G2000077405.

[1] J. K. Hwang *et al.*, Phys. Rev. C **67**, 054304 (2003).
[2] J. K. Hwang *et al.*, Phys. Rev. C **69**, 057301 (2004).
[3] Evaluated Nuclear Structure Data File, http://www.nndc.bnl.gov/ensdf
[4] S. Raman *et al.*, At. Data Nucl. Data Tables **36**, 1 (1987).
[5] G. Lhersonneau *et al.*, Z. Phys. A **351**, 357 (1995).
[6] D. C. Radford, Nucl. Instrum. Methods Phys. Res. A **361**, 297 (1995).
[7] H. Ohm *et al.*, Z. Phys. A **327**, 483 (1987).
[8] K.-L. Kratz *et al.*, Z. Phys. A **312**, 43 (1983).
[9] B. Pfeiffer and J. A. Pinston, private communication, 2003.
[10] J. Genevey, F. Ibrahim, J. A. Pinston, H. Faust, T. Friedrichs, M. Gross, and S. Oberstedt, Phys. Rev. C **59**, 82 (1999).
[11] Z. Berant *et al.*, Phys. Lett. **B156**, 159 (1985).
[12] G. Sadler *et al.*, KFA Ann. Rep., 1975, p. 87 (unpublished).
[13] K. Kawade *et al.*, J. Phys. Soc. Jpn. **55**, 1102 (1986).
[14] R. E. Sund *et al.*, Phys. Rev. C **10**, 853 (1974).

[15] R. G. Clark *et al*., in *Proceedings of the Third Symposium on Physics and Chemistry of Fission, Rochester, NY, 1973* (IAEA, Vienna, 1974), Vol. 2, p. 221.
[16] R. C. Jared *et al*., LBL-2366, 1974, p. 38 (unpublished).
[17] G. Mamane, Ph.D. thesis, Weizmann Institute of Science, Rehovot, Israel, 1983 (unpublished).
[18] E. Cheifetz *et al*., Phys. Rev. Lett. **25**, 38 (1970).
[19] E. Cheifetz *et al*., in *Proceedings Conference Nuclear Spectroscopy Fission Products, Grenoble, 1979*, edited by T. V. Egidy (Institute of Physics, Bristol, England, 1980), p. 193.
[20] E. Cheifetz *et al*., in *Proceedings Conference Nuclear Spectroscopy Fission Products, Grenoble, 1979*, p. 193 (1980).
[21] R. L. Watson *et al*., Nucl. Phys. **A141**, 449 (1970).
[22] A. G. Smith *et al*., Phys. Lett. **B453**, 206 (1999).
[23] V. E. Oberacker, A. S. Umar, E. Teran, and A. Blazkiewicz, Phys. Rev. C **68**, 064302 (2003).
[24] A. Blazkiewicz, V. E. Oberacker, A. S. Umar, and M. Stoitsov, Phys. Rev. C **71**, 054321 (2005).
[25] D. De Frenne and E. Jacobs, Nucl. Data Sheets **83**, 535 (1998).
[26] J. Kantele, *Handbook of Nuclear Spectrometry* (Academic, London, 1995).
[27] J. H. Hamilton, in *Treatise on Heavy Ion Science*, edited by A. Bromley (Plenum, New York, 1989), Vol. 8, p. 2.